Sources and fluxes of scale-energy in the overlap layer of wall turbulence

A. Cimarelli, E. De Angelis, P. Schlatter, G. Brethouwer, A. Talamelli and C.M. Casciola

Abstract

Direct Numerical Simulations of turbulent channel flows at friction Reynolds number 550, 1000, 1500, are used to analyse the turbulent production, transfer and dissipation mechanisms in the compound space of scales and wall-distances by means of the Kolmogorov equation generalized to inhomogeneous anisotropic flows. Two distinct peaks of scale-energy source are identified. The first stronger one belongs to the near-wall cycle. Its location in the space of scales and physical space is found to scale in viscous units while its intensity grows slowly with Re, indicating a near-wall modulation. The second source peak is found further away from the wall in the putative overlap layer and it is separated from the near-wall source by a layer of significant scale-energy sink. The dynamics of the second outer source appears to be strongly dependent on the Reynolds number. The detailed scale-by-scale analysis of this source highlights well-defined features that are used to make the properties of the outer turbulent source independent of Reynolds number and wall-distance by rescaling the problem. Overall, the present results suggest a strong connection of the observed outer scale-energy source with the presence of an outer region of turbulence production whose mechanisms are well separated from the near-wall region and whose statistical features agree with the hypothesis of an overlap layer dominated by attached eddies. Inner-outer interactions between the near-wall and outer source region in terms of scale-energy fluxes are also analysed. It is conjectured that the near-wall modulation of the statistics at increasing Reynolds number can be related to a confinement of the near-wall turbulence production due to the presence of increasingly large production scales in the outer scale-energy source region.

1 Introduction

One of the most peculiar aspects of turbulence in wall bounded flows is the ability of the turbulent fluctuations to regenerate themselves through self-sustained processes. In wall flows, the production of turbulent fluctuations is embedded in the system instead of being provided by an external agent. The dynamics of these self-sustaining mechanisms has been extensively investigated over the past thirty years, since these processes are responsible for the energy drain from

the mean flow to the fluctuating field and for the turbulent drag.

It has long been understood that the near-wall layer, being the site of the highest rate of turbulent energy production and of the maximum turbulent intensities, is crucial to the dynamics of attached shear flows. The possibility to identify robust kinematic features in the proximity of a wall fed the hope of the scientific community to obtain a complete and consistent dynamical description of the underlying physics of these processes. The turbulent fluctuations near a wall have been found to organize in well defined coherent motions consisting of quasi-streamwise vortices and high/low velocity regions alternating in the spanwise direction. The former are longitudinal vortices with typical streamwise and spanwise length scales $\lambda_x^+ \approx 200$ and $\lambda_z^+ \approx 50$, respectively (hereafter a superscript + will denote the so-called inner units, see e.g. Townsend [42]), slightly tilted away from the wall. The latter are long and wide alternating arrays of streamwise streaks of local velocity excess/defect, with length scales $\lambda_x^+ \approx 1000$ and $\lambda_z^+ \approx 100$, superimposed on the mean flow. These features have been recognized in several numerical and experimental works, see e.g. Kim *et al.* [22], Smith & Metzler [40] and Robinson [37]. From these observations, several scientists tried to derive a conceptual model of these processes. Following the work of Jiménez & Pinelli [21], the continuous creation and destruction of these turbulent structures form a self-sustaining cycle maintaining near-wall turbulence without the need of any input from the core flow, i.e. it is an autonomous cycle. The streamwise vortices extract energy from the mean flow to create alternating streaks of longitudinal velocity. Presumably by inflectional instabilities, these streaks in turn give rise to the vortices closing the cycle, see also Hamilton *et al.* [12], Jeong *et al.* [18], Schoppa & Hussain [39].

From a more applied point of view, the near-wall cycle is crucial since it controls the magnitude of the wall stress. But coherent structures exist also at larger scales in the so-called overlap layer [15, 14, 20], and have been recently suggested to form an outer self-sustaining mechanism of regeneration of very large turbulent fluctuations, see e.g. Flores & Jiménez [11], Mizuno & Jiménez [30], Hwang & Cossu [16]. The phenomenology resembles the self-regenerating cycle near the wall though its characteristic dimensions are larger, see e.g. Monty *et al.* [32], del Alamo *et al.* [10]. The coherent motions involved in this outer cycle should scale with external variables meaning that their dimensions and action should increase as the extent of the log-layer widens with Reynolds number. Hence, the understanding of these outer dynamics is crucial for the modeling of wall-turbulence in the asymptotic regime of very large Reynolds number. Furthermore, its analysis could help to clarify the interactions between the outer and inner regions of wall flows needed in the formulation of near-wall models for LES, see e.g. Piomelli & Balaras [36], and to explain the controversial mixed inner/outer scaling of the near-wall quantities such as spectra and turbulent intensities, see e.g. Hutchins & Marusic [15], DeGraaff & Eaton [8].

Generally speaking, the problem of wall-turbulent flows has been classically studied by dividing the flow domain into well characterized regions depending on wall-distance. In particular, wall-bounded flows are divided in a near-wall, inner region, and an outer region populated by large structures. These two dis-

tinct regions are present in all wall-bounded flows and interact in the overlap region. While in the outer flow the velocity profile depends on the particular flow configuration, in the inner and overlap regions it exhibits a high degree of universality starting linearly from the wall and then approaching a logarithmic behaviour. These behaviors opportunely scaled with viscous units should collapse for different flows and different Reynolds numbers, see Nagib & Chauhan [33] for a detailed description of the controversies on this topic. The same scaling should apply to the turbulent intensity profiles and to all the statistical observables of the inner region.

However, the near wall quantities exhibit a Reynolds dependence as shown by the fact that the energy of the long turbulent fluctuations of the overlap layer grows when the Reynolds number increases. This large-scale motion is found to actively modulate the near-wall turbulence by production of near-wall scales at increasing Reynolds number [15]. The observed increase of the streamwise turbulent fluctuation peak, the possible appearance of a second peak in the overlap flow and the presence of a marked outer-scale peak in the energy spectrum are thought to be a signature of these effects. An important consequence of the Reynolds number dependence of the large turbulent motion in the overlap layer is that most of the turbulence production should asymptotically come from this region due to the widening of the overlap layer with Re [41]. Even if no Reynolds dependence for the outer turbulent production intensity is expected, the outer turbulent self-sustained mechanisms are thought to dominate the high Reynolds number asymptotic state of wall turbulence.

Given the Reynolds dependence of these processes in the compound scale/physical-space, an interesting approach to study the basic mechanisms of the outer cycle has been recently proposed in Cimarelli *et al.* [6] by extending the statistical approach used in Marati *et al.* [26] and applied by Saikrishnan *et al.* [38] to moderately high Reynolds number data. The classical approach for addressing these issues in the channel flow is based on a Fourier decomposition along the homogeneous directions while keeping a description in terms of the physical distance in the wall normal direction, see e.g. del Alamo *et al.* [9]. However this more traditional approach does not allow for a net distinction between position in the wall normal direction and wall normal scale at which energy generation and energy flux take place. The tool used here to describe the energy content associated with a given scale of motion in a given position in space is based, instead, on the generalization of the Kolmogorov equation for the second order structure function, originally introduced for homogenous and isotropic turbulence, and successively extended to inhomogenous, anisotropic flows by Hill [13]. The generalized Kolomogorov equation keeps the two concepts of wall normal position and wall normal scale clearly distinct, thereby allowing to distinguish between the two associated components of the energy flux. In Cimarelli *et al.* [6], this multi-dimensional description of turbulence has been used and proven fundamental for the understanding of the wall-turbulent physics and for its modeling as shown in Cimarelli & De Angelis [3]. In the present paper, we extend this work by analysing how the turbulent energy associated to a certain scale (scale-energy) is generated, transferred and dissipated among different scales

3

Case	Re_τ	L_x	L_y	L_z	$N_x \times N_y \times N_z$	Δx^+	Δz^+
DNS550	550	$8\pi h$	$2h$	$4\pi h$	$1024 \times 257 \times 1024$	13.5	6.7
DNS1000	1000	$8\pi h$	$2h$	$3\pi h$	$2560 \times 385 \times 1920$	9.8	4.9
DNS1500	1500	$12\pi h$	$2h$	$10.5h$	$6144 \times 577 \times 3456$	9.2	4.5

Table 1: Parameters of the simulations. Re_τ is the friction Reynolds number, L_x, L_y and L_z are the lengths of the computational domain in the streamwise (x), wall-normal (y) and spanwise (z) direction, N_x, N_y and N_z are the number of points in physical space and Δ_x^+, Δ_y^+ and Δ_z^+ the corresponding grid spacing in viscous units.

and wall-distances varying the Reynolds number with particular attention to the outer self-regeneration mechanisms.

2 DNS database and single point statistics

In the present study, we analyze data of three direct numerical simulations (DNS) of fully developed turbulent channel flow at $Re_\tau = u_\tau h/\nu = 550$, 1000 and 1500 respectively. Here, u_τ is the friction velocity, h the channel half gap width and ν the viscosity. The simulations were carried out with a pseudo-spectral code using Fourier expansions and dealiasing in the homogeneous directions, and Chebyshev polynomials in the wall-normal direction. Full details of the algorithm can be found in Chevalier *et al.* [2]. The domain size and resolution of the three DNSs are given in table 1. Data of the DNSs at $Re_\tau = 550$ and 1000 have already been used for studies of wall-turbulence in Cimarelli *et al.* [6] and Lenaers *et al.* [23], respectively. Let us mention that the lower resolution adopted for the simulation of the lower Reynolds number case at $Re_\tau = 550$, has been tested and found to not affect the statistical quantities we are analysing in the present work.

Profiles of the streamwise mean velocity and the log-law indicator function of the three DNSs are shown in figure 1. The near-wall region has obviously a very high degree of similarity for the three Reynolds numbers, while outside the buffer layer, in the overlap layer, differences become visible due to Reynolds number effects. A tentative plateau in the indicator function profile starts to appear with increasing Re_τ but is not yet clearly present, meaning that a true logarithmic layer is absent even at the highest Re_τ.

The single-point turbulent kinetic energy balance compacts in a simple way the overall multidimensional behavior of turbulence describing the energetics only in physical-space. For the symmetries of the channel, this equation reads,

$$\frac{d\psi}{dy} = s(y) \ , \tag{1}$$

and describes how turbulent energy is redistributed among different wall-distances
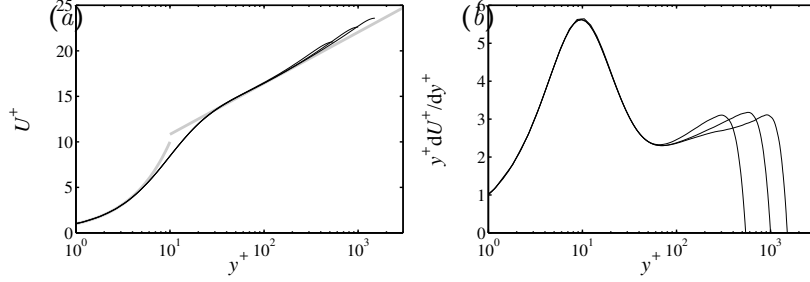
Figure 1: Mean velocity profiles $U^+(y^+)$ and (premultiplied) mean velocity gradient $y^+ \mathrm{d}U^+/\mathrm{d}y^+$ for the three channel DNS considered in this study, with $Re_\tau = 550, 1000, 1500$. $U^+(y^+) = y^+$ and $U^+(y^+) = 1/\kappa \log(y^+) + B$ with $\kappa = 0.41$ and $B = 5.2$ are indicated by thick gray lines.

y through the spatial flux $\psi = (\langle u_i^2 v \rangle + \langle pv \rangle /\rho - \nu d\langle u_i^2\rangle/dy)$ from the production to the dissipation regions of the flow defined by positive and negative values of the source term $s(y) = -\langle uv \rangle (dU/dy) - \langle \epsilon \rangle$. Hereafter, $\langle \cdot \rangle$ will be used to denote ensamble average. As shown by the black lines in figure 2(a), in wall-turbulence the energy source is near the wall in the so-called buffer layer. In this layer turbulence production exceeds the local dissipation. Conversely, the wall and bulk flow behave as sink regions dissipating turbulent energy emerging from the buffer layer through the spatial energy flux, see gray lines in figure 2(a). Indeed, the spatial flux is zero at the peak of energy source and becomes positive (towards the core flow) further away from the wall and negative (towards the wall) closest to the wall. Actually, in between the buffer layer and the core of the flow, a third region can be defined, the so-called overlap layer, which is the main subject of the present work. Although this region is expected to be an equilibrium layer where production and dissipation locally balance, production is actually larger than dissipation leading to an outer energy source, see figure 2(b). The understanding of this region of the flow is very important especially when dealing with the large Reynolds number state of wall-turbulence. Even if its intensity is very small compared to the one near the wall, this outer energy source shows an apparent Re-dependence, see again figure 2(b). In particular, it appears that by increasing the Reynolds number, the role of the outer energy source becomes more important. By defining the overall inner and outer energy source as the integral of the source $s(y)$ restricted to the two (inner and outer) regions where $s(y) > 0$, respectively,

$$\Xi_{inn} = \int_y s(y)dy \qquad y \in \{\text{inner region of energy source } s(y) > 0\}$$

$$\Xi_{out} = \int_y s(y)dy \qquad y \in \{\text{outer region of energy source } s(y) > 0\} \,,$$
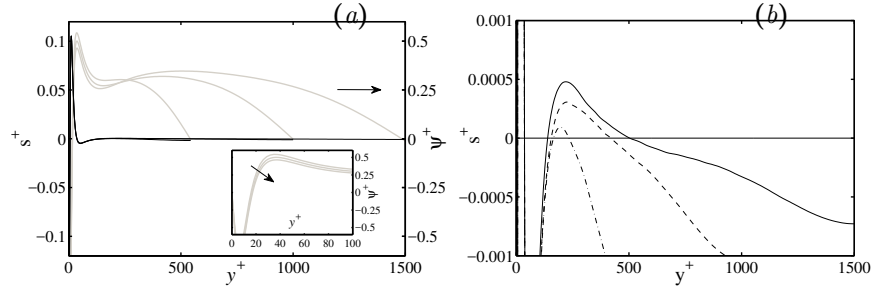
5

Figure 2: (a) Source term of the kinetic energy budget s^+ (black lines) and corresponding spatial flux ψ^+ (grey lines) for the three Reynolds numbers $Re_\tau = 550, 1000, 1500$. The inset shows a zoom of the near-wall peak of the spatial flux ψ^+. The two arrows indicate increasing Reynolds numbers. (b) Magnification of the region around the second positive peak of s. Increasing Re_τ from dash-dotted to dashed and solid lines.

we can roughly estimate the relative importance of the two regions as function of Reynolds number by means of the ratio Ξ_{out}/Ξ_{inn}. The present data show a significant increase of this ratio from 0.0031 at $Re_\tau = 550$ to 0.0347 and 0.0617 at $Re_\tau = 1000$ and 1500, respectively. Extrapolating this trend, one can expect the outer source to become dominant above $Re_\tau = 15000 \div 20000$. The increased intensity of the outer source has also consequences for the topology of the energy transfer. Indeed, as shown in figure 2(a), the spatial flux in the overlap layer increases with Re and forms an outer peak given by the increasing energy injection due to the outer energy source.

3 Generalized Kolmogorov equation

The generalized Kolmogorov equation proposed by Hill [13] is the balance equation for the second order structure function, $\langle \delta u^2 \rangle$, where $\delta u^2 = \delta u_i \delta u_i$ and the fluctuating velocity increment is $\delta u_i = u_i(X_s + r_s/2) - u_i(X_s - r_s/2)$. According to its definition, $\langle \delta u^2 \rangle(r_i, X_i)$ depends both on the separation vector defined as $r_i = x_i' - x_i$ and on the location specified by the mid-point $X_i = (x_i' + x_i)/2$. Hereafter, index repetition implies summation. The second order structure function can be interpreted as the amount of energy of a given scale r_s at a certain position in the flow X_s and for that reason, hereafter, we will refer to the concept of scale-energy. Let us note that, although $\langle \delta u^2 \rangle$ has the dimensions of kinetic energy and it is strictly related to the energy spectrum, the second order structure function is not an intensive quantity. However, it represents the natural tool for the multi-scale analysis of turbulent flows that lack a classical spectral decomposition due to violation of spatial homogeneity. The second order structure function is defined in a four-dimensional space (r_x, r_y, r_z, Y_c) allowing to distinguish fluxes between different wall-distances Y_c and fluxes between

6

different wall-normal scales r_y. This distinction would be missed by using the balance equation for spectral energy. The generalized Kolmogorov equation derives directly from the Navier-Stokes equations. For the symmetries of channel flow and considering increments r_s only in the directions parallel to the walls, $r_y = 0$, [26], the equation reads,

$$\frac{\partial \langle \delta u^2 \delta u_i \rangle}{\partial r_i} + 2 \langle \delta u \delta v \rangle \left(\frac{dU}{dy} \right)^* + \frac{\partial \langle v^* \delta u^2 \rangle}{\partial Y_c} =$$
$$-4 \langle \epsilon^* \rangle + 2\nu \frac{\partial^2 \langle \delta u^2 \rangle}{\partial r_i \partial r_i} - \frac{2}{\rho} \frac{\partial \langle \delta p \delta v \rangle}{\partial Y_c} + \frac{\nu}{2} \frac{\partial^2 \langle \delta u^2 \rangle}{\partial Y_c^2} . \qquad (2)$$

where $U(y)$ is the mean velocity profile, $Y_c = X_2$ is the wall-normal coordinate of the mid-point, (*) denotes the arithmetic average at the points $X_s \pm r_s/2$ and $\epsilon = \nu (\partial u_i / \partial x_j)(\partial u_i / \partial x_j)$ is the pseudo-dissipation. Equation (2) involves a four-dimensional vector field, $\mathbf{\Phi} = (\Phi_{r_x}, \Phi_{r_y}, \Phi_{r_z}, \Phi_c)$, and can be restated as

$$\nabla_4 \cdot \mathbf{\Phi}(\mathbf{r}, Y_c) = \xi(\mathbf{r}, Y_c) , \qquad (3)$$

where ∇_4 is the four-dimensional gradient and $\xi = -2 \langle \delta u \delta v \rangle (dU/dy)^* - 4 \langle \epsilon^* \rangle$ is the scale-energy source/sink given by the balance between production and dissipation. This equation allows to identify the two transport processes occurring simultaneously in wall-flows: the scale-energy transfer in the three-dimensional space of scales, $\mathbf{\Phi}_r = (\Phi_{r_x}, \Phi_{r_y}, \Phi_{r_z}) = \langle \delta u^2 \delta \mathbf{u} \rangle - 2\nu \nabla_r \langle \delta u^2 \rangle$ and the spatial energy flux among different wall-distances, $\Phi_c = \langle v^* \delta u^2 \rangle + 2 \langle \delta p \delta v \rangle / \rho - \nu/2 \partial \langle \delta u^2 \rangle / \partial Y_c$. In the inertial sub-range of homogeneous isotropic turbulence, eq.(3) reduces to

$$\nabla_3 \cdot \mathbf{\Phi}_r(\mathbf{r}) = -4 \langle \epsilon \rangle , \qquad (4)$$

where the contributions due to production, viscosity and spatial inhomogeneity are either negligible or zero. In this case, energy transport occurs only in the space of scales, is radial and from large to small scales. The scale-energy source, $\xi_{hom} = \langle \delta u \delta f \rangle - 4 \langle \epsilon \rangle$ where f is the external forcing, is a function only of the separation vector modulus $|\mathbf{r}|$ and it is always negative, $\xi_{hom} = g(|\mathbf{r}|) \leq 0$. In inhomogeneous flows, the turbulent production can locally exceed dissipation leading to regions of scale-energy source in the augmented $(\mathbf{r}, Y_c)$-space where $\xi(\mathbf{r}, Y_c) > 0$. This is a distinguishing feature of actual inhomogeneous flows that has been shown responsible in Cimarelli *et al.* [6] for a complex redistribution of scale-energy where the controversial reverse energy cascade plays a central role. Hence, in what follows, the study of the Reynolds number effects on the energetics of the flow will mainly focus on the behavior of the source term ξ.

4 The structure of the source term

The topological structure of the source term obtained from the three DNS data sets shows that all the basic characteristics observed at the lowest Re_τ are also maintained at higher Reynolds numbers. By analyzing the data in the reduced
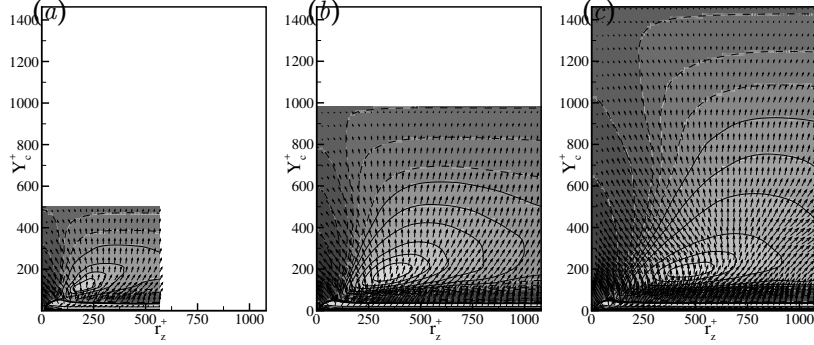
Figure 3: Direct numerical simulation of turbulent channel flows at $Re_\tau = 550$, $Re_\tau = 1000$ and $Re_\tau = 1500$ from left to right. Energy source – $\xi^+(r_x, r_z, Y_c)$ – isolines and field of fluxes – $(\Phi_{r_z}^+, \Phi_c^+)$ – vectors in the $r_x = 0$ plane. Energy source intensity increases from black to white colors. Solid lines denote postive values while dashed lines denote negative values.

space (r_x, r_z, Y_c) for $r_y = 0$, the source ξ is found to reach its maximum at $r_x = 0$ in a range of small spanwise scales well within the buffer layer, see figure 3. This region of the reduced space is a singularity point for the fluxes. As more clearly seen in figure 4, the scale-energy flux vector field takes origin from this peak of scale-energy source which can be considered as the engine of wall-turbulence and will be hereafter called the driving scale range (DSR). The small-scale location of the scale-energy source actually violates the classical paradigm of homogeneous isotropic turbulence. In wall flows, the turbulent energy is generated amid the spectrum of turbulent fluctuations, not at the largest scales, and this fact leads to a complex redistribution of energy [6], with strong consequences for turbulence modeling [4, 5].

Another interesting feature emerging from the analysis of the Kolmogorov equation is the existence of a rescaled replica of the DSR, associated with a second peak in the scale-energy source, called hereafter outer driving scale range (ODSR). This outer peak of scale-energy source has been observed in Cimarelli *et al.* [6] and is present also at higher Reynolds numbers, see the isocontours of figure 3.

4.1 The driving scale range DSR

In agreement with the picture of a universal near-wall region, the geometrical properties of the DSR are unaffected by the Reynolds number, see figure 4. For the three cases considered, the source peak within the DSR is located at $(r_x^+, r_z^+, Y_c^+) = (0, 40, 12)$. This Reynolds-number invariance and the clear matching of scales and positions suggests a strong connection with the near-wall cycle. Note that for a given wall-distance the source maximum ξ occurs
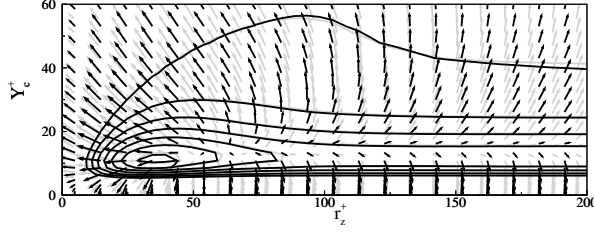
8

Figure 4: Scaling of the near-wall scale-energy source (ξ^+) and of the field of fluxes – $(\Phi_{r_z}^+, \Phi_c^+)$ in the $r_x = 0$ plane. Grey isolines and vectors denote the $Re_\tau = 1000$ case while black ones denote the $Re_\tau = 1500$ case.

at $r_x = 0$. Its location in the (r_z, Y_c)-plane, reported in figure 5(a), defines the typical spanwise scale of the scale-energy source, $(\ell_z^{\xi max})^+$. Near the wall, the spanwise location of the maxima increases quadratically with the wall distance, $(\ell_z^{\xi max})^+ \approx 35 + 0.02 Y_c^{+2}$, for all the Reynolds numbers considered. Clearly, within the DSR for small distances from the wall, $Y_c^+ < 30$, this trend results in an almost constant spanwise length scale: the typical spanwise scale of the most active structures of the wall is independent of the wall distance and Reynolds number. Although the topology of the DSR is basically Re-invariant, its intensity is not. The scale-energy source is found to slightly increase with Re_τ. In particular we measure $\xi_{max}^+ = 0.717, 0.732, 0.741$ moving from the lower to the higher Reynolds number. This trend is consistent with the commonly observed mixed inner/outer scalings of the near-wall quantities. In fact, it is thought that the outer dynamics actively modulates the near-wall turbulence by producing small scale fluctuations increasing Reynolds number [28].

As shown by the vector field in figure 4, a direct consequence of the Re-invariance of the topology of the scale-energy source term, ξ, is that also the scale-energy flux vector field, (Φ_{r_z}, Φ_c), remains identical for increasing Reynolds number, once rescaled in viscous units. In this scenario, the Reynolds-number effects should come only from the ODSR in the overlap region. Indeed, even if the observed second peak of scale-energy source ξ is very small compared to the one in the DSR, its relevance increases with Re as will be discussed in the next sections.

4.2 The outer driving scale-range ODSR

The ODSR belongs to the overlap layer and appears to be the result of a second outer turbulent production mechanism well separated from the near-wall dynamics. The ODSR is separated from the DSR by a scale-energy sink region. Interestingly, this separation is found to be more pronounced by increasing Re. The solid contour lines shown in figure 3, highlight that certain positive values for the source term ξ are shared by both the DSR and ODSR for the $Re_\tau = 550$. On the contrary, for the larger Reynolds numbers, the DSR and ODSR are more

9

and more separated by negative values for the source term ξ as shown by the number of dashed contours lines in between the inner and outer source shown in figure 3.

Although the peak intensity is smaller than the DSR one, the extent of the ODSR increases with Re suggesting how this object can play an important role at large Reynolds numbers. In contrast with the DSR where production is concentrated at small scales which are independent of Reynolds number, the ODSR involves larger scales and its extent in inner units increases with Re_τ. For the three Reynolds numbers considered, the peak of the ODSR occurs in a well-defined scale-region expressed in outer units corresponding to $r_z/h \approx 0.34$. On the other hand, the physical location of the peak in the ODSR is $Y_c/h = (0.2; 0.18; 0.12)$ in outer units while $Y_c^+ = (112; 186; 192)$ in viscous units going from low to the high Reynolds number. Contrary to the space of scales, r_z, which is found to be Re-invariant once expressed in outer units, the wall distances, Y_c, do not scale with Re neither in inner nor outer units. This behavior is probably related to the fact that the overlap layer extends from a lower limit given in viscous units to an upper limit in outer units, e.g. for $100 < Y_c^+ < 0.2Re_\tau$ but the exact values are still a matter of scientific debate, see Marusic *et al.* [28] and references therein. These arguments suggest a mixed scaling with wall-distance of the outer scale-energy source, see section 5 for a more detailed discussion. When considering the ODSR intensity, it is worth noting that the peak of scale-energy source in the ODSR remains essentially unaltered with Reynolds number once scaled in inner units and corresponds to $\xi^+ \approx 0.0095$.

The presence of the ODSR violates the equilibrium assumption of the overlap layer from which a local balance of production and dissipation is expected. Within the ODSR the energy injection is larger than the rate of dissipation, $\xi > 0$. As stated by equation (3), this fact results in a positive divergence of the energy transfer, $\nabla_4 \cdot \mathbf{\Phi} > 0$, which under the assumption of a true equilibrium is otherwise expected to be zero. This observation is consistent with the single-point energy excess already discussed in connection with figure 2 in section 2. Consequently, the overlap layer does not behave like a homogeneous shear flow traversed by a constant spatial flux of energy both at the single-point and two-point level. The ODSR continuously injects energy feeding the energy fluxes. As shown in figure 2, the spatial flux starts from the DSR in the buffer layer, it decreases by delivering energy in the sink layer wedged between the DSR and ODSR to increase again due to the energy injected by the ODSR leading to the second peak of the spatial flux. This second peak strongly depends on the Reynolds number, since the underlying physics of the ODSR belongs to the overlap layer whose extent and, hence, its overall energy injection, increases with Re, as figure 3 clearly suggests.

In this context, the existence of a simple near-wall viscous scaling may be questioned by the fact that different turbulent engines with different characteristic scales are at work thus leading to anomalous scaling. It is generally thought that the mixed inner/outer scaling is due to the fact that with increasing Reynolds number the large-scale structures of the overlap layer become more
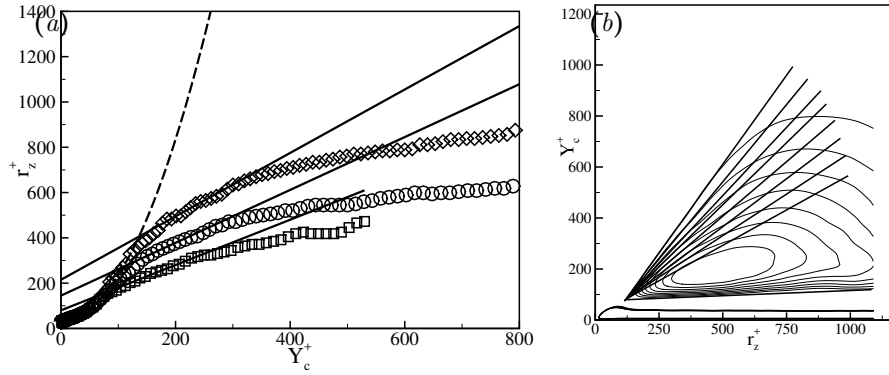
Figure 5: (a) Spanwise scale of maximum scale-energy source, $(\ell_z^{\xi max})^+$, as a function of the wall distance. Diamonds denote the $Re_\tau = 1500$ case, circles the $Re_\tau = 1000$ case and squares the $Re_\tau = 550$ case. The dashed line denotes the quadratic increase near the wall, $(\ell_z^{\xi max})^+ = 35 + 0.02 Y_c^{+2}$ while the solid lines the linear increase in the overlap layer, $(\ell_z^{\xi max})/h = 0.14 + (Y_c/h)$, $(\ell_z^{\xi max})/h = 0.14 + 1.16(Y_c/h)$ and $(\ell_z^{\xi max})/h = 0.14 + 1.4(Y_c/h)$, expressed in viscous units, i.e. $(\ell_z^{\xi max})^+ = 80 + Y_c^+$, $(\ell_z^{\xi max})^+ = 145 + 1.16 Y_c^+$ and $(\ell_z^{\xi max})^+ = 215 + 1.4 Y_c^+$. (b) Energy source $- \xi^+ -$ isolines in the $r_x = 0$ plane for the $Re_\tau = 1500$ case. The straight lines are $r_z^+ = \gamma(\xi_0^+)(Y_c^+ - \tilde{Y}_c^+) + \tilde{r}_z^+$ where ξ_0^+ defines the iso-level of ξ, $\gamma(\xi_0^+) \in [0.04, 1.4]$, $\tilde{r}_z^+ = 120$ and $\tilde{Y}_c^+ = 80$.

11

energetic and able to actively modulate the near-wall dynamics through production of near-wall fluctuations [15, 29, 28, 27]. Complementary to this picture, Jiménez [19] describes this modulation as a local effect where small-scales structures equilibrate with their large-scale environment. From a point of view of scale-energy source and transfer, the mixed inner/outer scaling of the near-wall region could be interpreted as the result of a confinement of the scale-energy excess emerging from the near-wall region due to the presence of increasingly large production scales in the overlap layer. At given Reynolds number, the scale-energy flux originated in the DSR and directed toward the bulk of the flow encounters the additional energy source given by the ODSR. This additional energy source radiates scale-energy and contributes to the overall energy flux. Below the ODSR the partial flux it generates is directed towards the wall, thereby opposing the flux produced in the DSR. The result is a net decrease in the flux towards the bulk. In fact, as stated by the turbulent kinetic energy and Kolmogorov equations (1) and (3), the source regions are repulsor for the fluxes. Increasing the Reynolds number, the DSR remains fixed when scaled in inner units, while the effect of the ODSR increases. As shown in figure 3, the fluxes deviate to try to avoid the ODSR which involves increasingly large scales with Re. Hence, the overall effect is a decrease with Reynolds number of the scale-energy flux from the near wall region due to the presence of increasingly large production scales with Re in the ODSR. Accordingly, in the inset of figure 2a a decrease of the near-wall peak of the single-point spatial flux is observed at increasing Re. This decrease is compared with the ratio between the overall outer and inner energy source, in figure 6. By increasing the Reynolds number, the ratio Ξ_{out}/Ξ_{inn} increases and, as a consequence, the near-wall peak of the single-point spatial flux, ψ_{max}^+, significanlty decreases. In conclusion, the scale-energy produced within the DSR increasingly feeds the turbulence in the near-wall region since the energy flux towards the channel center is decreasing with Re. The resulting growth of the energy available near the wall is, thus, responsible for intenser fluctuations with Re leading to a mixed inner/outer scaling of near-wall quantities.

5   Overlap layer scalings

Let us now investigate more in detail the peculiar features of the Kolmogorov equation within the overlap layer. The first point we address is the behavior with wall distance of the spanwise scale of maximum scale-energy source for a given wall-distance, $\ell_z^{\xi max}$. The present data show that for the three Reynolds number considered, $\ell_z^{\xi max}$ increases almost linearly with Y_c, see figure 5(a). In particular, we observe $(\ell_z^{\xi max})/h \approx 0.14 + (Y_c/h)$, $(\ell_z^{\xi max})/h \approx 0.14 + 1.16(Y_c/h)$ and $(\ell_z^{\xi max})/h \approx 0.14 + 1.4(Y_c/h)$ from low to high Reynolds numbers respectively. This behavior is similar to that reported in Saikrishnan *et al.* [38] for the shear scale L_s which is found to slightly increase its slope from $Re_\tau = 300$ up to $Re_\tau = 2000$ where it seems to asymptotically approach the dimensional prediction $L_s = ky$. Contrary to the slope, the intercept remains almost constant.
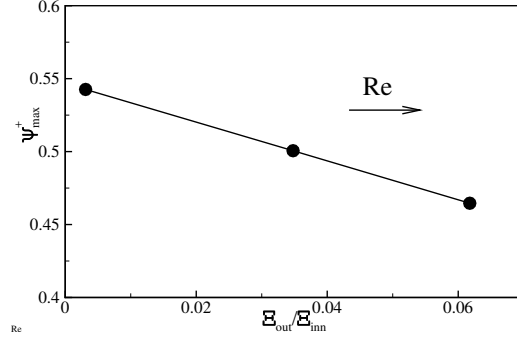
Figure 6: Behavior of the near-wall peak of the single point spatial flux, ψ^+_{max}, equation (1), as a function of the ratio Ξ_{out}/Ξ_{inn} for increasing Reynolds number.
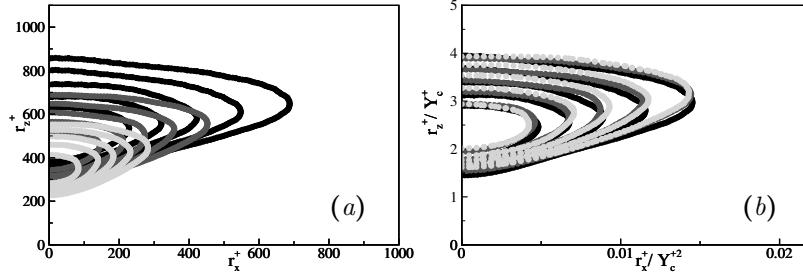

Figure 7: Scale-energy source isolines for three distances from the wall within the overlap layer for $Re_\tau = 1500$ ($Y_c^+ = 140$ light grey, $Y_c^+ = 180$ dark grey and $Y_c^+ = 220$, black). (a) In inner units the dimensions of the source region increase with the distance from the wall. In (b) spanwise and streamwise scales are normalized with the wall-normal distance and its square, respectively. Apparently, the isolines of the scale-energy source at different wall-normal distances tend to collapse one on top of the other.

13

This value of the intercept could be considered as the characteristic spanwise scale of the lower overlap layer. As shown by the isolines in figure 5(b) for $Re_\tau = 1500$, in the overlap layer the iso-levels of positive scale-energy source, $\xi > 0$, intercept spanwise scales which linearly increase with the distance from the wall. In particular, the iso-levels of ξ can be approximated by a sheaf of lines originating from a unique point at $\tilde{r}_z^+ = 120$ and $\tilde{Y}_c^+ = 80$ but with different slopes, i.e. $r_z^+ = \gamma(\xi_0^+)(Y_c^+ - \tilde{Y}_c^+) + \tilde{r}_z^+$ where ξ_0^+ defines the iso-level of ξ and $\gamma(\xi_0^+) \in [0.04; 1.4]$.

As already stated, the source maximum is found at $r_x = 0$ for all Y_c while for $r_x > 0$ the source decreases, see figure 7(a). By tracking the spanwise scale of the maximum of ξ as a function of the streamwise scale, we find that these spanwise scales increase following a square-root law, $r_z^+ \sim \sqrt{r_x^+}$, independently of the Reynolds number. This behavior is similar to that reported by del Alamo et al. [9] for the spectral distribution of the Reynolds stresses and it finds a possible theoretical explanantion in Moarref et al. [31] in terms of geometrically self-similar resolvent modes. Since we observe that the spanwise scales involved in the scale-energy source increase linearly with wall-distance, $r_z^+ \sim Y_c^+$, we argue that the streamwise scales should behave quadratically with wall-distance, i.e. $r_x^+ \sim Y_c^{+2}$. Hence, we expect the scale-space behavior of the scale-energy source of the ODSR in the overlap layer to be approximatively self-similar if plotted as function of r_x^+/Y_c^{+2} and r_z^+/Y_c^+. As shown in figure 7(b) this rescaling of ξ allows us for a unique comprhensive view of the outer scale-energy source where the Y_c-dependence is dropped. The data we have available at other Reynolds numbers (not shown) suggest that this behaviour is Re_τ independent. The comparison with figure 7(a) highlights that this single picture of the overall behavior of the outer scale-energy source would be missed when using viscous units. It is worth mentioning that the observed scale-space distribution of the outer scale-energy source, $r_z^+ \sim Y_c^+$ and $r_x^+ \sim Y_c^{+2}$, is consistent with the energy distribution found in Moarref et al. [31] which, although different from the original scaling proposed by Townsend [42], is explained by the conjecture of an overlap layer populated by self-similar structures attached to the wall, see e.g. del Alamo et al. [10].

We address now the possibility to scale also the intensity of the outer scale-energy source, $\xi = -2\langle \delta u \delta v \rangle (dU/dy)^* - 4\langle \epsilon^* \rangle$. The rate of viscous dissipation is constant in the space of scales and can be easily modeled by means of the equilibrium hypothesis, $\langle \epsilon \rangle \sim u_\tau^3/\kappa y$. On the contrary, the scale-dependent behaviour of the production intensity is not trivial and need a detailed analysis. Two distinct regimes are expected whose transition should be controlled by the shear scale ℓ_S [17]. For scales larger than ℓ_S the prevailing mechanism which determines the scaling law is production. For scales smaller than ℓ_S, the energy cascade prevails and an isotropy-recovering behavior is expected to occur. This range should be characterized by a power law with universal exponents based on the dimensional predictions proposed by Lumley [25]. As shown in figure 8(a) for $Re_\tau = 1500$ (the same behavior is observed also for the lower Reynolds numbers considered), the scale-energy production follows the classical Lumley's
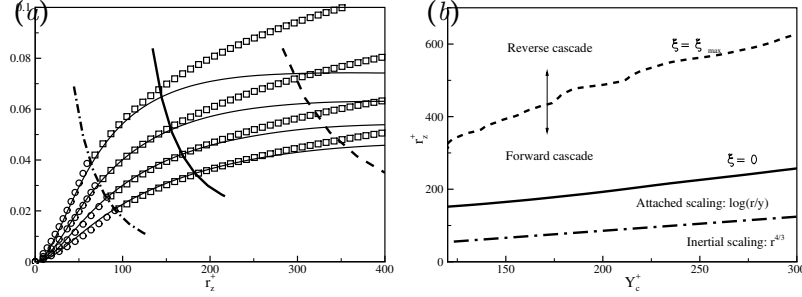
Figure 8: (a) Scaling of production, $-2\langle\delta u\delta v\rangle(dU/dy)$, for $r_x = 0$ and $Re_\tau = 1500$. From top to bottom the four solid lines provide the production at $Y_c^+ = 130$, 160, 190 and 230, respectively. Squares denote the logarithmic behavior described by equation (6) and circles denote the inertial behavior, equation (5). The three thick lines show the characteristic scales reported in (b). (b) Y_c-behavior of the scale of maximum scale-energy source, $(\ell_z^{\xi_{max}})^+ \approx 215 + 1.4Y_c^+$ (dashed line) and of the zero scale-energy source, $(\ell_z^{\xi_{zero}})^+ \approx 80 + 0.65Y_c^+$ (solid line). The shear scale, $\ell_S^+ = \kappa Y_c^+$ (dashed-dotted line), represents the cross-over between logarithmic and power law scaling of production.

prediction for the mixed structure function [25, 17], here extended to scale-energy production by taking into account the mean shear, dU/dy,

$$-2\langle\delta u\delta v\rangle\frac{dU}{dy} = \beta u_\tau^3(r/y)^{4/3}/\kappa y \qquad \text{for} \qquad r < \kappa y\,, \qquad (5)$$

where κ is the von Kármán constant, see circles in figure 8(a). Production follows this power law for scales smaller than the shear scale ℓ_S as shown by the thick dashed-dotted line in figure 8(a). The shear scale defined as $\ell_S = \sqrt{\epsilon/S^3}$ where $S = dU/dy$, is computed here by using the overlap layer estimate, $\ell_S = \kappa Y_c$. Hence, the power law (5) is valid for scales smaller than the distance from the wall, the so-called *detached* scales. At scales larger than ℓ_S (*attached* scales), we find that the production in the overlap layer is well described by a logarithmic law,

$$-2\langle\delta u\delta v\rangle\frac{dU}{dy} = u_\tau^3(C + D\log(r/y))/\kappa y \qquad \text{for} \qquad \kappa y < r < \ell_z^{\xi_{zero}}\,, \qquad (6)$$

squares in figure 8(a). This law is closely related to the (k^{-1})-law for the energy spectrum derived by Perry *et al.* [35], see also Nikora [34]. As shown in Davidson *et al.* [7], the real space analogue of the (k^{-1})-law is a logarithmic law for the streamwise second-order structure functions. Equation (6) represents an extention of this law to the mixed structure functions, $\langle\delta u\delta v\rangle$, which takes into account also the mean shear, dU/dy. Scaling (6) remains valid up to $r_z = \ell_z^{\xi_{zero}}$ where $\ell_z^{\xi_{zero}}$ is defined as the scale where the source term becomes zero, $\xi = 0$.
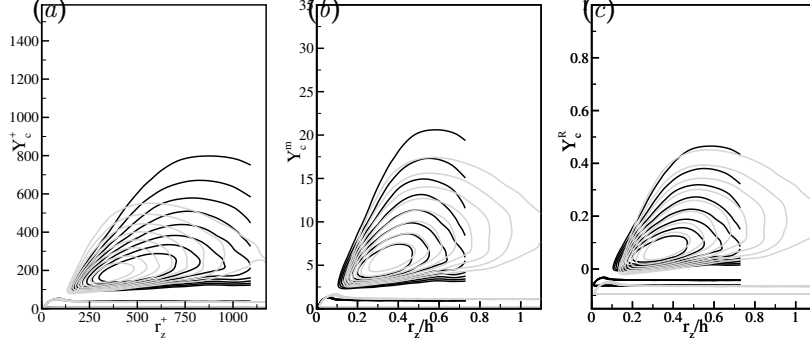
Figure 9: Energy source – ξ^+ – isolines in the $r_x = 0$ plane for $Re_\tau = 1000$ (grey) and $Re_\tau = 1500$ (black). In (a) ξ^+ is shown as a function of viscous quantity, (r_z^+, Y_c^+), in (b) as a function of mixed quantity, $(r_z/h, Y_c^m)$, and in (c) as a function of rescaled quantity, $(r_z/h, Y_c^R)$.

For scales smaller than $\ell_z^{\xi_{zero}}$ the source term is actually a sink for the scale-energy fluxes, $\xi < 0$, while for larger scales it is a source, $\xi > 0$.

According to equation (3) and as shown by the vector field in figure 3, scales smaller than $\ell_z^{\xi_{zero}}$ are characterized by a negative divergence of the fluxes since $\xi < 0$ and, thus, by a forward cascade. As a consequence, the logarithmic behavior (6) is associated with turbulent scales involved in a forward cascade process. Since, as anticipated, these scales are larger than $\ell_S = \kappa Y_c$ they are influenced by the presence of the walls. On the other hand, the power law scaling characterizes scales smaller than $\ell_S = \kappa Y_c$. Hence, the influence of the wall should be somehow negligible and, consequenlty, the forward cascade should resemble the classical one proposed by Kolmogorov since an isotropic recovery should start to take place, see Casciola *et al.* [1]. It could be worth stressing that the shear scale, often identified with the distance from the wall, has been longly addressed to explain the momentum and energy transfer between different scales of motion, starting from the pioneering work of Townsend [42] to more recent contributions, see e.g. Nikora [34] and Lozano-Duran & Jiménez [24]. As shown in figure 8(b), both ℓ_S and $\ell_z^{\xi_{zero}}$ linearly increase with the wall distance denoting again statistical features attached to the wall. Since the slope of $\ell_z^{\xi_{zero}}$ is larger than that of the shear scale, ℓ_S, we can expect that the range of scales where the logarithmic scaling holds, should expand significantly with Reynolds number increasing the importance of the scaling for the prediction of production.

Figure 5 suggests a possible approximation for the source term for scales larger than $\ell_z^{\xi_{zero}}$. By assuming that the production term for scales close to $\ell_z^{\xi_{max}}$ roughly behaves linearly with r_z, see figure 8, we can model the source term as $\xi^+ \approx A(Y_c^+)r_z^+ + B(Y_c^+)$ since dissipation is a scale-independent process. In addition, we have also found in section 4.2 that the iso-levels of $\xi > 0$ form a

16

sheaf of lines described by the equation, $r_z^+ = \gamma(\xi_0^+)(Y_c^+ - \tilde{Y}_c^+) + \tilde{r}_z^+$ where ξ_0^+ defines the iso-level of ξ we are considering, see figure 5. By combining these two informations, the slope γ is given by $\gamma(\xi_0^+) \approx G\xi_0^+ + H$, implying that the source term can be approximated as $\xi^+ \approx (r_z^+ - \tilde{r}_z^+)/G(Y_c^+ - \tilde{Y}_c^+) - H/G$. From our data we find $G = 103.9$ and $H = 0.58$.

Summarizing, we have shown that for a fixed Reynolds number the complex multidimensional features of the ODSR can be described in a simple way by using the self-similarity of the streamwise and spanwise scales shown in figure 7 and the scaling of the production intensity shown in figure 8. Despite the limited range of Reynolds numbers we have available, let us address now how this picture changes for different Reynolds numbers. As already shown in section 4.2, the intensity of the outer scale-energy source scaled in viscous units and its scale-space location scaled in outer units remain constant for the present Reynolds numbers. Hence, the effect of Reynolds number mainly reduces to an expansion/shrinking of the wall-normal distances. A sufficiently general procedure could be to consider a mixed scaling of the wall-normal distance in the form $Y_c^m = (Y_c/h)^\alpha (Y_c^+)^\beta$. Alternatively one could use outer units shifting the origin according to the expression $Y_c^R = (Y_c/h) - \eta^+/Re_\tau$ where η^+ is a free parameter. By considering $\alpha = \beta = 1/2$ in the first case and $\eta^+ = 100$ in the second one, the resulting scaling of the outer scale-energy source is shown in figure 9. Although not conclusive given the small range of Reynolds numbers investigated this result seems to be consistent with the possibility of a universal rescaling of the outer scale-energy source (ODSR).

6   Concluding remarks

By means of the description of turbulence given by the generalized Kolmogorov equation we study the scale-energy transfer and production mechanisms of turbulent wall flows at different Reynolds numbers. Two driving mechanisms in terms of scale-energy source are identified for the fluxes. The first stronger one, the driving-scale range DSR, belongs to the near-wall cycle. As expected, its inner-scaled topology remains unaltered with Reynolds while its intensity is found to slightly increase with Re (near wall modulation). The second outer scale-energy source, outer driving scale range ODSR, takes place further away from the wall in the overlap layer and is separated from the DSR by a distinct scale-energy sink layer suggesting a possible independence of the production mechanisms of the ODSR from the near-wall region which might be interpreted as an autonomous outer cycle. Although its intensity is small compared to the DSR, the outer region of scale-energy source expands with Reynolds number while its peak intensity remains almost constant. These observations suggest the importance of the ODSR for large Reynolds number wall-turbulence.

Further analysis of the ODSR demonstrates that the Re-dependence of the outer scale-energy source can be dropped by scaling in outer units the space of scales and in mixed one the wall-distance at least for the range of Reynolds numbers analysed here. Furthermore, we found that the spanwise scales involved in

the scale-energy source linearly increase with the distance from the wall. On the other hand, the streamwise scales are connected to these spanwise scales of scale-energy source through a square root law and, hence, quadratically increase with wall distance. These observations allow us to scale the outer scale-energy source highlighting its self-similarities for different wall distances and Reynolds numbers. While considering the intensity of the outer scale-energy source, we found that the space of scales within the overlap layer can be divided into two distinct ranges. For scales larger than the shear scale, ℓ_s, but smaller than the cross-over scale of zero scale-energy source, $\ell_z^{\xi_{zero}}$, the outer scale-energy source follows a logarithmic law, $\xi = u_\tau^3(C + D\log(r/y) - 1)/\kappa y$. This behavior is theoretically consistent with the presence of a k^{-1} law for the energy cospectrum. For scales smaller than the shear scale, the outer scale-energy source follows a power law whose exponent equals Lumley's dimensional prediction, $\xi = u_\tau^3(\beta(r/y)^{4/3} - 1)/\kappa y$. These scales are involved in a direct cascade whose features should resemble the classical one since they are detached from the wall and, hence, an isotropic recovery is expected to take place. Interestingly, both $\ell_z^{\xi_{zero}}$ and ℓ_s increase linearly with wall distance. The different increase with wall-distance of these two scales highlights the possible extention of the range of scales of validity of the logarithmic law for the prediction of outer scale-energy source at large Reynolds numbers. Overall, these observations suggest a strong connection of the observed outer scale-energy source with the presence of an outer turbulence production cycle whose statistical features agree with the hypothesis of an overlap layer dominated by self-similar structures attached to the wall.

The topology of the energy transfer is also studied. The paths of energy resembles the one reported in Cimarelli *et al.* [6] for a lower Reynolds number case. Only one singularity point related to the DSR exists from which the fluxes depart also for larger Reynolds number. According to our observations we may expect a high Reynolds number state of wall-turbulence where only one origin for the fluxes exists and corresponds to the DSR at the small-scales of the near-wall region, since the intensity of the ODSR should be substantially Re-independent. In this scenario, the Reynolds number effects on the energy transfer should come only from the expansion of the ODSR both in scale and physical space with Re. For increasing Reynolds numbers, the turbulent energy emerging from the DSR near the wall experiences an expanding outer scale-energy source in the overlap layer which acts as a repulsor for the fluxes as stated by equation (3). Hence, the fluxes try to avoid the increasingly large production scales of the ODSR and remain partially confined to the wall-region increasing the overall amount of energy locally available near the wall. Accordingly, we observe a decrease of the spatial flux from the buffer to the overlap layer at increasing Reynolds numbers. Hence we may conjecture that the near-wall modulation is a result of a confinement of the near-wall source due to the presence of increasingly large production scales in the overlap layer.

References

[1] CASCIOLA, C.M., GUALTIERI, P., JACOB, B. & PIVA, R. 2005 Scaling properties in the production range of shear dominated flows. *Phys. Rev. Lett.* **95** (024503).

[2] CHEVALIER, M., SCHLATTER, P., LUNDBLADH, A. & HENNINGSON, D.S. 2007 SIMSON - a pseudo-spectral solver for incompressible boundary layer flows. *Tech. Rep.* TRITA-MEK 2007:07. KTH Mechanics, Stockholm, Sweden.

[3] CIMARELLI, A. & DE ANGELIS, E. 2011 Analysis of the Kolmogorov equation for filtered wall-turbulent flows. *J. Fluid Mech.* **676**, 376–395.

[4] CIMARELLI, A. & DE ANGELIS, E. 2012 Anisotropic dynamics and subgrid energy transfer in wall-turbulence. *Physics of Fluids* **24** (1), 015102.

[5] CIMARELLI, A. & DE ANGELIS, E. 2014 The physics of energy transfer toward improved subgrid-scale models. *Phys. Fluids* **26**, 055103.

[6] CIMARELLI, A., DE ANGELIS, E. & CASCIOLA, C.M. 2013 Paths of energy in turbulent channel flows. *J. Fluid Mech.* **715**, 436–451.

[7] DAVIDSON, P.A., NICKELS, T.B. & KROGSTAD, P.A. 2006 The logarithmic structure function law in wall-layer turbulence. *J. Fluid Mech.* **550**, 51–60.

[8] DEGRAAFF, D.B. & EATON, J.K. 2000 Reynolds-number scaling of the flat-plate turbulent boundary layer. *J. Fluid Mech.* **422**, 319–346.

[9] DEL ALAMO, J.C., JIMÉNEZ, J., ZANDONADE, P. & MOSER, R.D. 2004 Scaling of the energy spectra of turbulent channels. *J. Fluid Mech.* **500**, 135–144.

[10] DEL ALAMO, J.C., JIMÉNEZ, J., ZANDONADE, P. & MOSER, R.D. 2006 Self-similar vortex clusters in the turbulent logarithmic region. *J. Fluid Mech.* **561**, 329–358.

[11] FLORES, O. & JIMÉNEZ, J. 2006 Effect of wall-boundary disturbances on turbulent channel flows. *J. Fluid Mech.* **566**, 357–376.

[12] HAMILTON, J.M., KIM, J. & WALEFFE, F. 1995 Regeneration mechanisms of near-wall turbulence structures. *J. Fluid Mech.* **287**, 317–348.

[13] HILL, R.J. 2002 Exact second-order structure-function relationship. *J. Fluid Mech.* **468**, 317–326.

[14] HUTCHINS, N. & MARUSIC, I. 2007 Evidence of very long meandering streamwise structures in the logarithmic region of turbulent boundary layers. *J. Fluid Mech.* **579**, 1–28.

[15] HUTCHINS, N. & MARUSIC, I. 2007 Large-scale influences in near-wall turbulence. *Phil. Trans. R.Soc. A* **365**, 647–664.

[16] HWANG, Y. & COSSU, C. 2010 Self-sustained process at large scales in turbulent channel flow. *Phys. Rev. Lett.* **105**, 044505.

[17] JACOB, B., CASCIOLA, C.M., TALAMELLI, A. & ALFREDSSON, H.P. 2008 Scaling of mixed structure functions in turbulent boundary layers. *Phys. Fluids* **20** (045101).

[18] JEONG, J., HUSSAIN, F., SCHOPPA, W. & KIM, J. 1997 Coherent structures near the wall in a turbulent channel flow. *J. Fluid Mech.* **332**, 185–214.

[19] JIMÉNEZ, J. 2012 Cascades in wall-bounded turbulence. *Annu. Rev. Fluid Mech.* **44**, 27–45.

[20] JIMÉNEZ, J. & HOYAS, S. 2008 Turbulent fluctuations above the buffer layer of wall-bounded flows. *J. Fluid Mech.* **611**, 215–236.

[21] JIMÉNEZ, J. & PINELLI, A. 1999 The autonomous cycle of near-wall turbulence. *J. Fluid Mech.* **389**, 335–359.

[22] KIM, H.T., KLINE, S.J. & REYNOLDS, W.C. 1971 The production of turbulence near a smooth wall in a turbulent boundary layer. *J. Fluid Mech.* **50**, 133–160.

[23] LENAERS, P., LI, Q., BRETHOUWER, G., SCHLATTER, P. & ÖRLÜ, R. 2012 Rare backflow and extreme wall-normal velocity fluctuations in near-wall turbulence. *Phys. Fluids* **24**, 035110.

[24] LOZANO-DURAN, A. & JIMÉNEZ, J. 2014 Time-resolved evolution of coherent structures in turbulent channels: characterization of eddies and cascades. *J. Fluid Mech.* **759**, 432–471.

[25] LUMLEY, J.L. 1965 Interpretation of time spectra measured in high-intensity shear flows. *Phys. Fluids* **8**, 1056.

[26] MARATI, N., CASCIOLA, C.M. & PIVA, R. 2004 Energy cascade and spatial fluxes in wall turbulence. *J. Fluid Mech.* **521**, 191–215.

[27] MARUSIC, I, MATHIS, R & HUTCHINS, N 2010 Predictive model for wall-bounded turbulent flow. *Science* **329**, 193–196.

[28] MARUSIC, I., McKEON, B.J., MONKEWITZ, P.A., NAGIB, H.M., SMITS, A.J. & SREENIVASAN, K.R. 2010 Wall-bounded turbulent flows at high reynolds numbers: Recent advances and key issues. *Phys. Fluids* **22**, 065103.

[29] MATHIS, R., HUTCHINS, N. & MARUSIC, I. 2009 Large-scale amplitude modulation of the small-scale structures of turbulent boundary layers. *J. Fluid Mech.* **628**, 311–337.

[30] MIZUNO, Y. & JIMÉNEZ, J. 2013 Wall turbulence without walls. *J. Fluid Mech.* **723**, 429–455.

[31] MOARREF, R., SHARMA, A.S., TROPP, J.A. & MCKEON, B.J. 2013 Model-based scaling of the streamwise energy density in high-reynolds-number turbulent channels. *J. Fluid Mech.* **734**, 275–316.

[32] MONTY, J.P., STEWART, J.A., WILLIAMS, R.C. & CHONG, M.S. 2007 Large-scale features of turbulent pipe and channel flows. *J. Fluid Mech.* **589**, 147–156.

[33] NAGIB, H.M. & CHAUHAN, K.A. 2008 Variations of von Karman coefficient in canonical flows. *Phys. Fluids* **20**, 101518.

[34] NIKORA, V. 1999 Origin of the "-1" spectral law in wall-bounded turbulence. *Phys. Rev. Lett.* **83**, 734–736.

[35] PERRY, A.E., HANBEST, S.M. & CHONG, M.S. 1986 A theoretical and experimental study of wall turbulence. *J. Fluid Mech.* **165**, 163–199.

[36] PIOMELLI, U. & BALARAS, E. 2002 Wall-layer models for large-eddy simulations. *Annu. Rev. Fluid Mech.* **34**, 349–374.

[37] ROBINSON, S.K. 1991 Coherent motions in the turbulent boundary layer. *Annu. Rev. Fluid Mech.* **23**, 601–639.

[38] SAIKRISHNAN, N., DE ANGELIS, E., LONGMIRE, E.K., MARUSIC, I., CASCIOLA, C.M. & PIVA, R. 2012 Reynolds number effects on scale energy balance in wall turbulence. *Phys. Fluids* **24**, 015101.

[39] SCHOPPA, W. & HUSSAIN, F. 2002 Coherent structure generation in near-wall turbulence. *J. Fluid Mech.* **453**, 57–108.

[40] SMITH, C.R. & METZLER, S.P. 1983 The characteristics of low speed streaks in the near wall region of a turbulent boundary layer. *J. Fluid Mech.* **129**, 27–54.

[41] SMITS, A.J., MCKEON, B.J. & I., MARUSIC. 2011 High-reynolds number wall turbulence. *Annu. Rev. Fluid Mech.* **43**, 353–375.

[42] TOWNSEND, A.A. 1976 *The Structure of Turbulent Shear Flow*. Cambridge University Press.